A piezoelectric transducer made of biodegradable materials – design and properties

AGNIESZKA MIRKOWSKA^{1*}©, PIOTR RYTLEWSKI²©, NATALIA PUSZCZYKOWSKA²©, MICHAŁ SOŁOGUB¹

¹Department of Electrical Engineering Fundamentals, Wroclaw University of Science and Technology pl. Grunwaldzki 13, 50-377 Wroclaw, Poland

²Faculty of Materials Engineering, Kazimierz Wielki University ul. Chodkiewicza 30, 85-064 Bydgoszcz, Poland

e-mail: *agnieszka.mirkowska@pwr.edu.pl, {prytlewski/nat}@ukw.edu.pl, 266063@student.pwr.edu.pl

Abstract: In the paper, the construction and properties of a layered piezoelectric transducer made of biodegradable materials are presented. The transducer consists of an electret layer, an elastic coating, and an outer structural layer. As the electret layer, the polylactide (PLA) foil with a thickness of 20 µm was used. The electrical properties of the foil, such as resistivity, relative permittivity, and charge decay, were examined. The elastic coating was made of natural rubber (NR), ensuring flexibility, while the outer structural layer was fabricated from PLA using a 3-D printing method. Two different shapes of the PLA-grid were examined: hexagonal and striped, to evaluate their influence on the electromechanical performance of the device. In the paper, the model and electro-mechanical properties of the transducer are presented. The electret foil was polarized using a high-voltage corona charging method. The maximal value of the piezoelectric coefficient, possible to obtain, was calculated using the described model, and it is equal to $d_{33\text{MAX}} = 1.4 \text{ nC/N}$ for a hexagonal structure and 0.87 nC/N for a striped one. That corresponds to the maximal value of effective charge density $q_{sMAX} = 7.9 \text{ mC/m}^2$ limited by Paschen's law. The measured static value of the piezoelectric coefficient d_{33} was up to 280 pC/N. The presented results demonstrate the potential of biodegradable piezoelectric transducers for sustainable and environmentally friendly applications in energy harvesting and sensor technologies.

Key words: biodegradability, biodegradable transducer, electret, piezoelectric transducer, polylactide

1. Introduction

The increasing social awareness regarding the green transition leads to searching for solutions that enable the replacement of petroleum-based polymer materials with biodegradable alternatives. This also applies to piezoelectric materials, which are used in biomedical applications [1, 2] energy harvesting [3], wearable electronics [4], or large-scale piezoelectric transducers such as sleep sensors [5]. The variety of applications imposes the development of transducers with demanding requirements, including geometry, sensitivity, elasticity, acoustic impedance, or biocompatibility. The natural and synthetic biodegradable piezoelectric polymers

exhibit finite piezoelectric properties, such as: chitosan ($d_{33} \approx 18$ pC/N) glycine ($d_{33} \approx 5$ pC/N) [6] and synthetic biodegradable piezoelectric polymers such as: polylactic acid PLA ($d_{14} \approx 20$ pC/N [7]), polyhydroxybutyrate PHB ($d_{33} \approx 3$ pC/N), and other [1]. Moreover, the piezoelectric properties of those polymers are strictly correlated with their molecular structure and intrinsic dipole alignment, and the symmetry of the piezoelectric effect is low.

However, higher piezoelectric coefficients are possible to obtain in sandwich-like structures [8]. The maximal reported value of such sandwich-like structures reaches even 22 nC/N [9]. Those structures involve at least two main layers: thin electret materials, which are dielectrics exhibiting a quasi-permanent electric charge, and an elastic layer made of material characterized by high flexibility, such as thermoplastic polyurethane TPU [10] or elastomers [11]. The piezoelectric response of those materials is limited by geometrical dimensions, Young's modulus of the elastomer layer, and the effective charge density of electret foil [1–16]. The application

Generally, the dielectrics with high volume resistivity such as polypropylene (PP), fluoropolymers: polytetrafluoroethylene (PTFE, FEP), polyethylene (HDPE, LDPE, XLPE or polyethylene terephthalate (PET) are typically examined for their electret properties. Due to their high bulk resistivity of about $10^{16} \Omega m$, the Maxwell-time constant is approximately at a level of more than 54 h, which can assume a long charge-life time [14]. Experimental results show that electret materials' charge-life time reaches years [15]. Moreover, they can be applied in the form of gaseous-solid composites, so-called ferroelectrets, or piezoelectrets [8, 9]. Those foam-like, open-voided cellular structures are characterized by large piezoelectric response, flexibility, and low acoustic impedance. The piezoelectric coefficient d_{33} reaches about 800 pC/N [18]. The main disadvantage is the complex prefabrication process of such cellular-like structures, including stretching and foaming [19].

The main disadvantage of the mentioned dielectrics is their decomposition time, which is much longer than their technical usefulness, causing problems with waste storage of electret-based products. Thus, electret materials originating from fossil fuels can be replaced with biodegradable alternatives such as polylactide (PLA), characterized by high dielectric resistivity up to $10^{15} \Omega m$ [18, 19]. The PLA composites with montmorillonite [22], talc, and mica [23] or proteinase K [24] were also examined. The piezoelectric coefficient d_{33} for foamed PLA ferroelectret reaches even $d_{33} = 300 \text{ pC/N}$) [25].

Moreover, the parts of sandwich-like piezoelectric structures, or even whole transducers, can be 3-D printed using PLA filament [4, 11, 12, 26, 27] This method of prefabrication of the whole transducer, or its particular components, is low-cost and allows for adjusting the geometric dimensions for particular applications.

In this paper, the piezoelectric transducer in the form of a sandwich-like structure with a metal ring is presented. Particular layers of the described transducer are biodegradable, excluding metal electrodes. The electro-mechanical properties of particular layers and whole transducers are examined, and the results are discussed. Unlike previously mentioned designs [13, 15], the biodegradable elastic coating made of natural rubber is applied. The model for both hexagonal-shaped and striped-shaped structures is described, and the piezoelectric coefficient d_{33} is calculated and compared with experimental results. Implementation of the presented model

allows for predicting the piezoelectric response of the whole transducer due to the geometric, electric, and mechanical properties of particular layers.

2. Transducer model and construction

2.1. Transducer model

According to Fig. 1, the perpendicular external force F makes the 'soft' layer (1) compressed (Δx), leading to the deformation of the charged (with effective charge density q_s) foil (2) into a dielectric mesh (3). Therefore, the change in dimension f causes the induction of a charge on the rigid electrode (4), occurring as a change of voltage ΔU . That leads to the presence of a piezoelectric response.

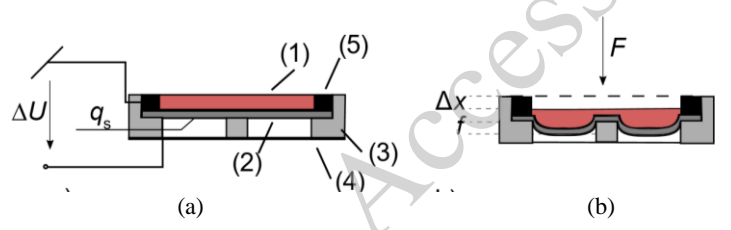


Fig. 1. (a) Construction of a piezoelectric transducer containing (1) – elastic coating called a 'soft' top layer, (2) – one-sided metalized biodegradable foil with effective charge density q_s deposited on the other side of the foil, (3) dielectric base with perforated dielectric mesh in the bottom, (4) – rigid electrode, (5) – ring electrode and (b) simplified strain distribution under external force F, where Δx is the deformation of elastomer layer and f – maximum deformation of electret foil

In [12], the model for the calculation of the piezoelectric coefficient d_{33} for closed round voids (see Fig. 2) was presented. The theory of Kirchhoff-Love for a thin, round plate was assumed. As stated in [12], the well-known two-layer model of piezoelectric non-uniform structures can be applied to calculate the coefficient d_{33} for the whole structure [22] only if the given relation is in power:

$$K_{fH} = \frac{(1-v^2)}{128} \cdot \frac{S_2}{S_1} \cdot \frac{l^4}{k_2^3} \cdot \frac{Y_{eff}}{Y_p} \cdot \frac{1}{x} > 1, \tag{1}$$

where K_{fH} is the mechanical factor for hexagonal-void structure, v is the Poisson's constant of the foil, S_2 is the area of gas-electret interphase, $S_2 = S - S_1$ (see Fig. 2), x_2 is the thickness of the foil, l is the diameter of the gas void, effective Young's modulus Y_{eff} of the 'soft' top layer, x is the thickness of the 'soft' top layer.

$$d_{33} = \frac{K_e \cdot \frac{S_2}{S_1} \cdot q_S}{Y_e},\tag{2}$$

where q_s is the effective charge density deposited on electret foil, S_2 is the area of gas-electret interphase, $S_2 = S - S_1$, where S is the whole area of the electret foil, Y_e is the Young's modulus of natural rubber, and K_e is the factor dependent on the geometry and electrical properties of particular layers as follows:

$$K_e = \frac{x_1 x_2 \varepsilon_1 \varepsilon_2}{(x_1 \varepsilon_2 + x_2 \varepsilon_1)^2},\tag{3}$$

where x_1 is the thickness of a gas layer for a structure without external stress, x_2 is the thickness of the electret foil, ε_1 is the electric permittivity of a gas, ε_2 is the electret permittivity of an electret foil. The K_e coefficient reaches its maximum value $K_{e\text{MAX}} = 0.25$ when the relation $x_{1\varepsilon 2} = x_{2\varepsilon 1}$ is fulfilled [28].

In this paper, not only is the hexagonal void-shaped structure investigated, but also the stripped one. The cross sections of the dielectric meshes are presented in Fig. 2.

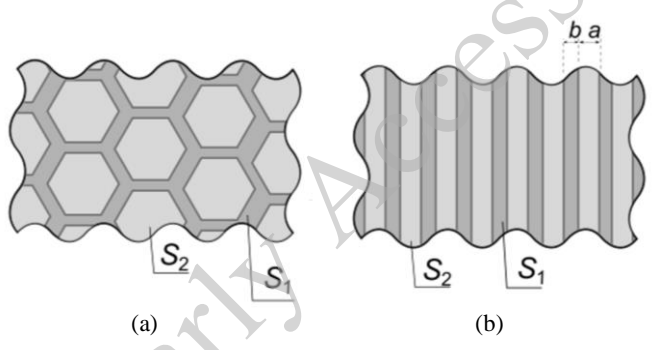


Fig. 2. Cross sections of: (a) hexagonal and (b) stripped dielectric meshes, where S_1 and S_2 are the areas of solid dielectric-electret and gas-electret interphase, respectively, and the a and b parameters are the widths of gas-electret interphase and dielectric-electret interphase, respectively

For the stripped-void structure, the $\Delta x Lb$ (L is the length of the void, b is the width of the dielectric-electret interphase, see Fig. 2) is the volume of the deformed elastomer layer, and $1/2\pi Lfa$ is the volume of the collapsed foil with cross-section in the form of a half ellipse, where f (the maximum deformation of the foil) is given for the rectangular plate as [29]:

$$f = \frac{pa^4}{64D} = \frac{pa^4}{64} \cdot \frac{12(1-\nu^2)}{Y_n x_n^3},\tag{4}$$

where p is the applied pressure, D is the flexural rigidity for the rectangular thin plate, Y_p is the Young's modulus of the PP foil, a is the width of the gas void, x_2 is the thickness of the foil, v is the Poisson's constant of the foil. Thus, the relation for the mechanical factor for the stripped structure K_{fS} will differ from Eq. (1) and is given below:

$$K_{fS} = \frac{3\pi(1-\nu^2)}{256} \cdot \frac{S_2}{S_1} \cdot \frac{a^4}{x_2^3} \cdot \frac{Y_{eff}}{Y_p} \cdot \frac{1}{x} \cdot \frac{a}{b} > 1.$$
 (5)

2.2. Transducer construction

In this study, a layered piezoelectric transducer design is proposed, with layers made of biodegradable materials, as presented in Fig. 3. The dielectric base with perforated dielectric mesh (1) is prefabricated using 3-D printed technology. The PLA filament (Avtek, Poland) was applied with Flashforge Adventurer 3 PRO printer.

The brass metal ring (3) was applied to provide stabilization of the electret foil (2). Moreover, it ensures the electrical connection between the transducer and measuring equipment. Then, as the electret layer (2), the PLA foil with a thickness of $x_2 = (20 \pm 1) \, \mu \text{m}$ was used with a graphite electrode (graphit conductive coating, Kontakt Chemie).

The PLA films were extruded from polylactide (PLA) in the form of grains with dimensions of $150{\text -}300~\mu\text{m}$ (Luminy® PLA LX 175, Total-Corbion, Gorinchem, The Netherlands). The grade melt flow ratio is 3~g/10~min (2.16~kg, 190°C) and a density is $1.24~g/\text{cm}^3$. For film prefabrication, the laboratory processing line consisting of a Plasti-Corder PLV 151 single-screw extruder (Brabender, Duisburg, Germany) was applied. The temperature of the heating zones was controlled at the level of 180°C . The rotational speed of the screw was $20{\text -}40~\text{revs/min}$ [30].

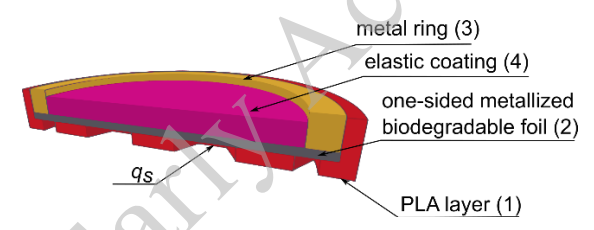


Fig. 3. Transducer cross-section, where (1) – 3D printed outer PLA layer, (2) – one-sided metalized biodegradable foil with corona charged effective charge density q_s , (3) – metal ring, (4) – NR elastic layer

Moreover, biodegradable natural rubber (NR) was used as an elastic coating (2). The thickness of the layer is (3.25 ± 0.05) mm, and the Young modulus is 3.0 MPa.

Two different shapes of dielectric mesh layer were prepared: hexagonal (H) and striped (S), as presented in Fig. 4. The projects were prepared using Tinkercad software. The height of the mesh is $x_1 = 2$ mm for both (hexagonal and striped structures).

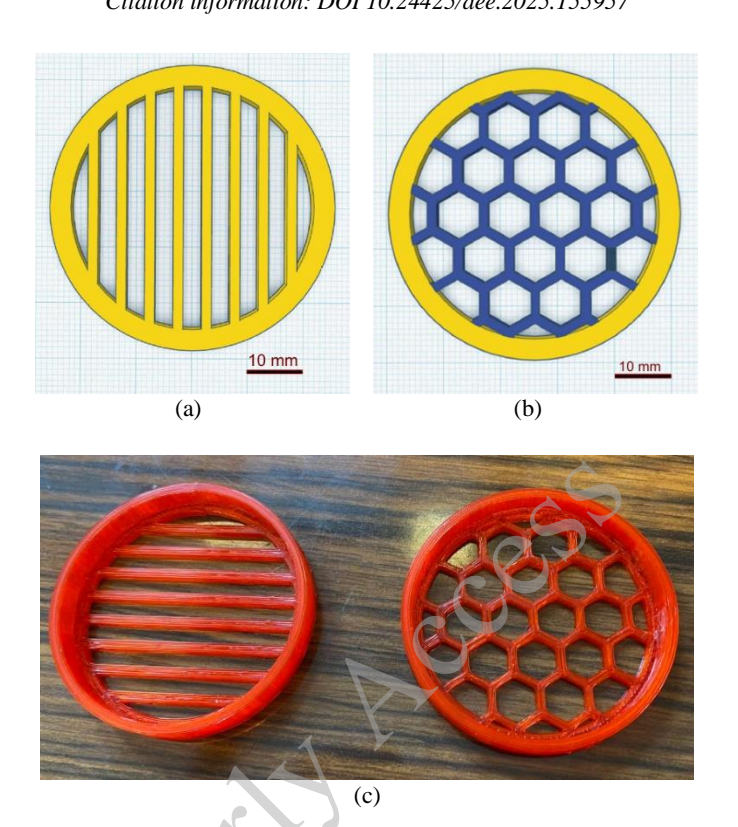


Fig. 4. Top view of model of PLA 3-D printed dielectric layers, where: (a) model with striped-void shape (S); (b) model with hexagonal-void shape (H); (c) photo of real samples

2.3. Transducer properties calculations

The S_2/S coefficient differs due to the selected structure, and for the hexagonal structure, it is 0.71, but for the striped, it is only 0.5, the a/b = 1. The Poisson's coefficient for the PLA foil is 0.35. The calculated values of mechanical factors are $K_{fH} \approx 1900$ and $K_{fS} = 165 > 1$. Thus, the relation given in Eq. (2) could be applied for the calculation of d_{33} parameter.

Due to Townsend's model of Paschen's breakdown and assuming that the atmospheric pressure p is equal to 1013 hPa with the height of the gas void $x_2 = 2$ mm, the maximum value of effective charge density reaches $q_{\rm sMAX} = 7.9 \, {\rm mC/m^2}$ [17, 26]. The maximum value of the piezoelectric coefficient $d_{\rm 33MAX}$ can be calculated as:

$$d_{33\text{MAX}} = \frac{K_e \frac{S_2}{S_1} \cdot q_{s\text{MAX}}}{Y_e}.$$
 (6)

For a hexagonal-void structure, the calculated $d_{33\text{MAX}H}$ is 1377 pC/N, and for square one, $d_{33\text{MAX}S} = 871$ pC/N.

3. Methods

3.1. Sample activation - corona charging process

The setup presented in Fig. 5 was used to activate PLA foil with dimensions of 70×70 mm with a graphite electrode. The sample (5) was placed in Faraday's cage (3) on the grounded electrode (6) at a distance of $h_c = 30\pm 1$ mm under the needle electrode (4), which was supplied by the DC high voltage power supply DORA ± 20 kV (1).

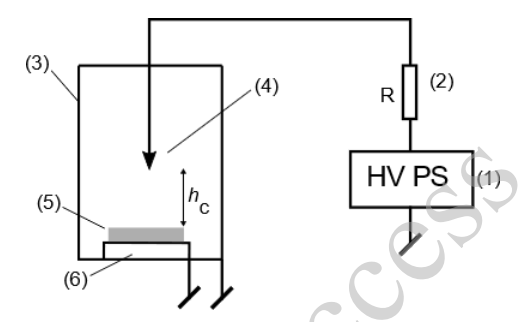


Fig. 5. Setup for corona poling of samples, where: (1) – high voltage power supply, (2) – limiting resistor $R = 2.2 \text{ M}\Omega$, (3) – Faraday's cage, (4) – needle high voltage electrode, (5) – sample, (6) – grounded electrode

The applied charging voltage for PLA foil was $U_c = -11$ kV for time $t_c = 30\pm1$ s.

3.2. Effective charge density and charge decay measurements

The setup for indirect effective charge density and charge decay measurements is presented in Fig. 6. For equivalent voltage measurements, sample (1) was placed in position a) on the grounded electrode at a distance of 15 ± 1 mm under the needle electrode, which was supplied by the DC high voltage power supply TREK $610E \pm 10$ kV (5). In position b), the equivalent voltage was measured using the electrostatic voltmeter TREK 347 (3) with the dedicated electrostatic probe TREK 6000B (4) placed at a distance of 2 mm above the sample (see Fig. 6(b)).

This paper has been accepted for publication in the AEE journal. This is the version, which has not been fully edited and content may change prior to final publication.

Citation information: DOI 10.24425/aee.2025.155957

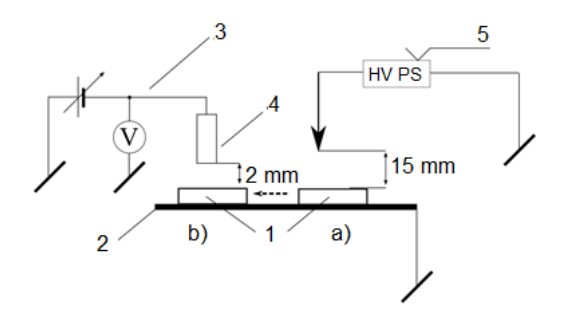


Fig. 6. Setup for equivalent voltage measurements, where: (1) – sample, (2) – grounded measuring table, (3) – electrostatic meter, (4) – electrostatic probe, (5) – high voltage power supply

The equivalent voltage measurements were performed under the following conditions: charging time $t_c = (30 \pm 1)$ s; air temperature $(22 \pm 1)^{\circ}$ C; relative air humidity $w = (24 \pm 2)$. The effective surface charge density q_s can be related with the equivalent voltage by the relation:

$$q_s = \varepsilon_0 \varepsilon_2 \frac{u_z}{x_2},\tag{7}$$

where Uz is the measured equivalent voltage, ε_2 is the electric permittivity of the PLA foil, $\varepsilon_0 = 8.85 \cdot 10^{-12}$ F/m is the vacuum permittivity, x_2 is the thickness of the electret foil. The effective charge density q_s is stored in the electret foil is highly dependent on the poling voltage U_c and the properties of the foil [7, 27].

Three different samples of PLA foil were examined, as presented in Table 1.

No.	Material name	Length × width, mm	Thickness	Poling voltage Uz
1.	PLA foil	35 × 35	20 μm	-5 kV/+6 kV/-6 kV
2.	PLA filament	35 × 35	1 mm	+6 kV
3.	PLA foil + hexagonal mesh	70 × 70	20 μm/0.5 mm	−11 kV*

Table 1. Samples used for charge decay measurements

The charge distribution along the x and y axes was examined for a 2-layer sample made up of two layers: initially charged PLA foil and hexagonal mesh with a thickness of 0.50 ± 0.05 mm, about 30 minutes after the charging process.

3.3. Resistivity and dielectric permittivity measurements

The information about bulk resistivity ρ_{ν} and relative dielectric permittivity ϵ_2 of the material is necessary for Maxwell-time constant calculation, as follows:

^{* -} The setup presented in Fig. 5 was used for charging according to the dimensions of the sample

This paper has been accepted for publication in the AEE journal. This is the version, which has not been fully edited and content may change prior to final publication.

Citation information: DOI 10.24425/aee.2025.155957

$$\tau_{Me} = \varepsilon_0 \varepsilon_2 \rho_v, \tag{8}$$

where $\varepsilon_0 = 8.85 \cdot 10^{12}$ F/m is the vacuum permittivity.

The cross-resistance measurements were carried out in accordance with PN-EN-61340-2-3 standard using the Resistance Meter, TREK Model 152-1 with dedicated electrodes: Trek Model 152P-CR-1 Probe. The cross-resistance measurements were performed under the following conditions: measurement voltage $U_p = 100 \pm 1 \text{ V}$; measurement time $t_p = 60 \pm 1$ s; air temperature 22 ± 1 °C; relative air humidity $w = 24 \pm 2$ %. The bulk resistivity ρ_{ν} was calculated from 5 cross-resistance R_{ν} measurements using the following relation:

$$\rho_v = R_v \cdot \frac{\pi (d_1 + g)^2}{x_2},\tag{9}$$

where $d_1 = 30.5 \pm 1$ mm is the inner contact electrode diameter, g = 13.25 mm is the distance (gap) between contact electrodes, x_2 is the thickness of the sample.

The dielectric permittivity and dielectric loss factor $tg\delta$ measurements were carried out in a 2-electrode system (the diameter of the sample was d = 25 mm) in accordance with PN-86/E-04403 standard. The sample was inserted inside Faraday's cage, and the capacitance and dielectric loss factor was measured by 3522-50 LCR HiTester by HIOKI. The ε_2 was calculated using the following equation [33]:

$$\varepsilon_2 = \frac{c_x - c_b - c_r}{c_0},\tag{10}$$

where C_x is the measured capacity, C_0 is the geometrical capacity calculated as:

the dispersion capacitance
$$C_r$$
 as:
$$C_0 = 6.95 \cdot 10^{-12} \frac{d^2}{x_2}, \tag{11}$$

$$C_r = 0.177 \cdot d \cdot 10^{-10}, \tag{12}$$

$$C_r = 0.177 \cdot d \cdot 10^{-10},\tag{12}$$

and the edge capacitance C_b as:

$$C_b = \pi d(-5.8 \cdot \log x_2 - 8.7) \cdot 10^{-12}. \tag{13}$$

3.4. Static piezoelectric coefficient measurements

The arrangement previously described in [15, 29] for measuring the piezoelectric coefficient d_{33} was used. The weight of the measuring electrode of diameter 20 mm was 52 g, which corresponds to an initial load of 1.6 kPa. The piezoelectric coefficient d_{33} could be easily calculated from the relation:

$$d_{33} = \frac{\Delta U \cdot C_T}{\Delta m \cdot g},\tag{14}$$

where $C_T = 1.596 \pm 0.029$ nF is the measured total capacitance of the whole measuring system, ΔU is the voltage change measured by electrometer RFT 6302 (average of 10 measurements,

reading made 5 seconds after load application), induced by the change of sampling load: $\Delta m = 200 \text{ g}$, $g = 9.81 \text{ m/s}^2$ is the gravitational acceleration. The voltage pulses were registered using Tektronix TDS 1002B oscilloscope.

4. Results and discussion

4.1. Maxwell time constant calculation

The measured cross-resistance (average from 5 measurements) of the PLA foil is $3.3 \cdot 10^{12} \Omega$, and according to Eq. 5, the bulk resistivity of the applied PLA foil is $2.5 \times 10^{14} \Omega m$. The dielectric permittivity ε_2 and dielectric loss factor $tg\delta$ change in function of frequency as presented in Fig. 7.

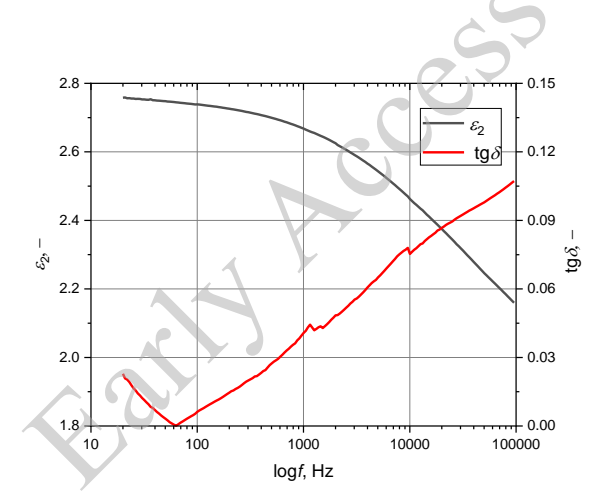


Fig. 7. Changes of dielectric permittivity ε_2 and dielectric loss factor $tg\delta$ of PLA foil due to applied frequency in the range from 20 Hz to 100 kHz

The dielectric permittivity $\varepsilon_w = 2.66$ for a frequency equal to 1 kHz. Due to Eq. (5), the Maxwell-time constant can be calculated, and it is equal to 1.6 h for the PLA. In Table 2, the comparison of electrical parameters between the examined PLA and well-known electret materials is presented [6, 30].

Table 2. Selected properties of electret materials and Maxwell-time constant calculations

Material	Dielectric constant ε _w	Bulk resistivity ρ_{v} , Ω m	Maxwell-time constant τ_{Me} , h
PLA	2.66	$2.5 \cdot 10^{14}$	1.56
PTFE	2.1	10^{17}	516

PP	2.4	10^{16}	59
PET	2.6	10^{16}	64

The Maxwell-time constant for the examined PLA is by an order of magnitude lower than for well-known electret materials, which is related to lower bulk resistivity in comparison to PTFE or PP (see Table 2).

4.2. Charge decay measurements

For comparison to the data presented in Table 2, the Maxwell-time constant for materials can also be estimated using charge-decay characteristics. The exemplary equivalent voltage characteristics, or corresponding surface charge decay characteristics, are presented in Fig. 8.

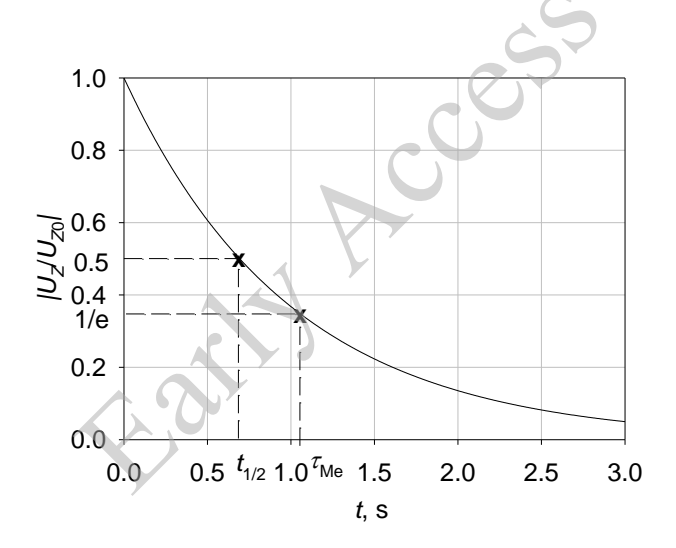


Fig. 8. The exemplary equivalent voltage $U_Z = f(t)$ time characteristic with marked Maxwell-time constant τ_{Me} and half-decay time $t_{1/2}$, the data is presented in relative values referred to U_{Z0} – initial value of equivalent voltage for t = 0.

The value of the Maxwell-time constant can be determined by measuring the time at which the initial value of effective charge density decreases to 1/e of its initial value. This relationship is strictly valid only for an exponential charge decay. Since charge decay in electret materials usually follows different curves, charge stability is typically characterized for comparison purposes using the so-called half-decay time $t_{1/2}$. The half-decay time $t_{1/2}$ is defined as the time at which the effective charge density q_s (or the equivalent voltage U_Z) decreases to half of its initial value.

The summary results of charge-decay measurements are presented in Table 3.

This paper has been accepted for publication in the AEE journal. This is the version, which has not been fully edited and content may change prior to final publication.

Citation information: DOI 10.24425/aee.2025.155957

Initial voltage Charging Half-decay time **Maxwell-time** Material voltage U constant τ_{Me} , h $U_{\rm Z0}$, kV $t_{1/2}$, h +5 -5 1.420 2.68 3.57 PLA foil +6 1.994 2.60 3.85 2.606 0.60 2.03 -6PLA fila-1.705 +6 1.69 ment

Table 3. Properties of materials

The half-decay time was read directly from experimental data (see Fig. 8). The Maxwell-time constant for the examined samples was calculated using exponential approximation:

$$U_Z(t) = A \exp(-Bt). \tag{15}$$

The fitting exponential coefficients A and B and the coefficient of determination R^2 are presented in Table 4.

Table 4. The fitting exponential coefficients A and B and the coefficient of determination R^2 fitted for charge decay curves

Charging voltage U_e	A	<i>-B</i> ⋅10 ⁻⁵	R^2
-5	1168	5.391	0.93
+6	1615	5.645	0.92
-6	1731	9.549	0.87

As given in Table 4, the determination R^2 is lower than 0.95, so the fitting of the curves is not sufficiently accurate, but it allows for estimation of the values of the Maxwell-time constant. The initial values of equivalent voltage U_{Z0} are higher (see Table 3) than the estimated ones (see Table 2). It should also be noted that the Maxwell-time constant estimated using charge-decay measurements is higher than the Maxwell-time constant calculated using Eq. 5 [7, 27]. Different curves, such as multiple-term power series models, could be applied for better fitting [12].

The Maxwell-time constant for the PLA calculated using measured curves (see Table 3) is higher than calculated using Eq. (8), equal to 1.6 h. Similar properties are described for PTFE, where calculated Maxwell-time constants are days (see Table 2), but the results show that it could reach years. The calculations of Maxwell-time constant using permittivity and resistivity are not always corresponding due to a variety of mechanisms leading to the charge decay as stated in [15].

As presented in Fig. 9, the Maxwell-time constant and $t_{1/2}$ are highly dependent on polarity and the value of the charging voltage U_e .

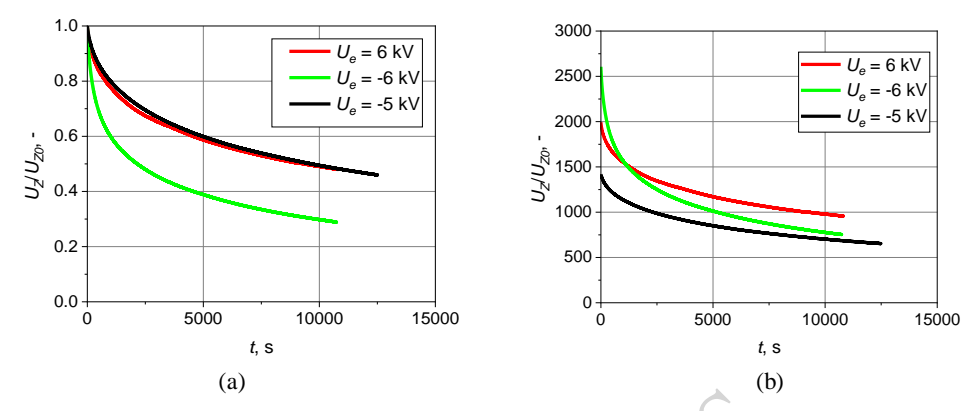


Fig. 9. Time-dependence of the equivalent voltage of PLA foil in (a) relative units and (b) absolute units for different charging voltages U_e

Moreover, the crossover phenomenon, well-known for polyethylene charge-decay curves, is observed [36]. The research on the electret properties of PLA should be developed, leading to a greater understanding of PLA nature and the possibilities to apply PLA as an electret material.

4.3. Equivalent voltage distribution

In Fig. 10, the equivalent voltage distribution on a charged PLA foil with 3-D printed PLA mesh with hexagonal voids of the thickness of 0.50 mm is presented. The measurements were taken about 30 minutes after charging. The results are averaged by measuring the aperture of the applied probe.

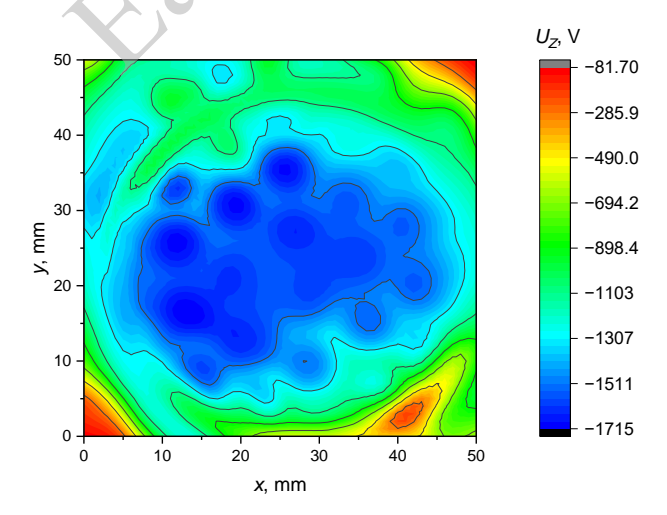


Fig. 10. Equivalent voltage distribution on charged PLA foil with 3-D printed PLA mesh with hexagonal mesh on it

The distribution confirms assumptions made in the model that only the effective charge density stored on the gas-electret interphase is responsible for the piezoelectric response of the structure. The influence of PLA foil – PLA mesh interphase (area S_1) on the distribution of electric field and charge decay can be further investigated.

4.4. Static piezoelectric coefficient d_{33}

The voltage pulses generated by regularly applying and removing the load are presented in Fig. 11. The oscilloscope image was registered for a hexagonal-shaped structure for initial pressure p = 1.6 kPa.

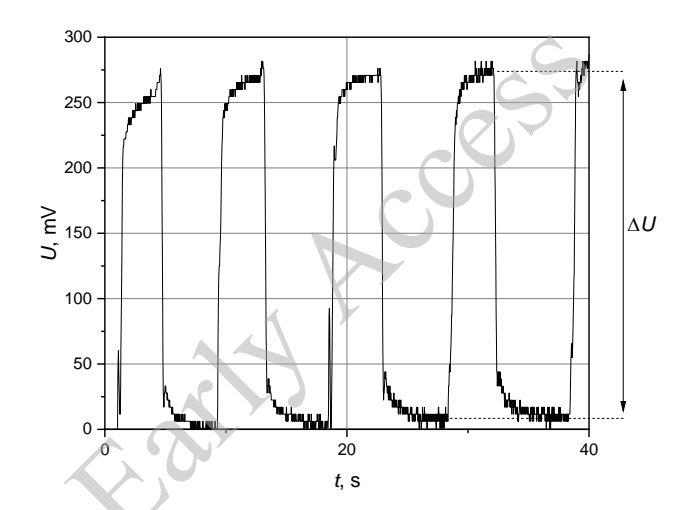


Fig. 11. Static pressure dependence of piezoelectric coefficient d_{33} for both hexagonal (d_{33H}) and striped (d_{33S}) structures

In Fig. 12, the static pressure dependence of the piezoelectric coefficient d_{33} for both hexagonal (d_{33H}) and striped (d_{33S}) structures is presented. The fitted curves and determination coefficients, R^2 , are also located in the Fig. 12.

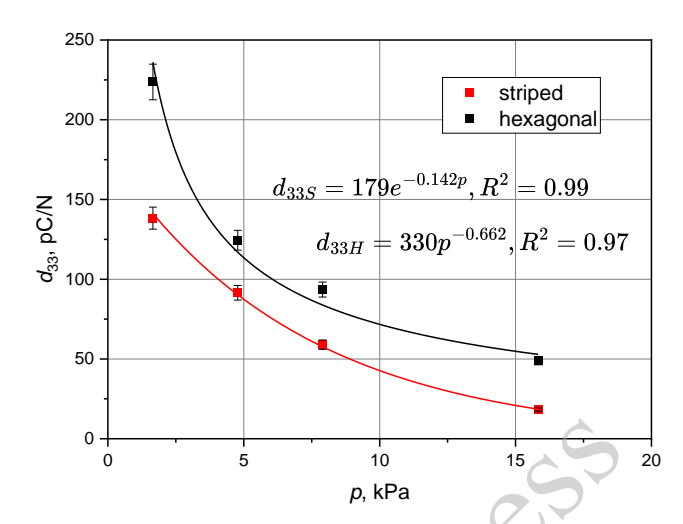


Fig. 12. Static pressure dependence of piezoelectric coefficient d_{33} for both hexagonal (d_{33H}) and striped (d_{33S}) structures

The piezoelectric response for both structures is highly pressure-dependent, which was previously noticed [12]. This phenomenon can be explained by non-linearities in the stress-strain function of natural rubber, like for other high elastic materials [10]. Anyway, the dynamics of the characteristics are different. The power function was fitted for the hexagonal structure as it was previously presented [12], but for the striped structure, the exponential curve seemed to be a better match. In Table 5, the comparison of measured and calculated piezoelectric coefficients is presented.

Table 5. The comparison of the measured and calculated piezoelectric coefficient

Sample type	d _{33MAX} , pC/N	d _{33m} , pC/N	d ₃₃ , pC/N	d_{33}/d_{33m} , %
Hexagonal	1377	262	224±11	85
Striped	871	166	138±7	83

The $d_{33\text{MAX}}$ is the maximal value of the coefficient calculated using Eq. (6), assuming the $q_{s\text{MAX}} = 7.9 \text{ mC/m}^2$. According to Fig. 10, the equivalent voltage 30 minutes after charging is $U_Z \cong 1700 \text{ V}$, which corresponds to an effective charge density equal to $q_s = 1.5 \text{ mC/m}^2$ (see Eq. (7)). Substituting into Eq. (6), the calculated piezoelectric coefficient d_{33m} is 262 pC/N for the hexagonal structure and 166 pC/N for the striped structure. These results correspond to measured values of d_{33} equal to 224 pC/N and 138 pC/N, respectively. The d_{33m} is about 5 times lower than $d_{33\text{MAX}}$, which is caused by differences in effective charge density q_s measured 30 minutes after foil charging, and the calculated maximal value of charge density $q_{s\text{MAX}}$. Increasing the charging voltage is possible to obtain higher effective charge densities; however, the range

of the used probe is 3200 V (see Section 3.2), and another probe should be applied to widen the measurement range and further model validation.

Table 6. The comparison of the piezoelectric coefficient d_{33} for a hexagonal-shaped structure for different times after charging

Time after charging	30 minutes	4 days	1 month
d ₃₃ , pC/N	224 ± 11	56 ± 6	52 ± 3

Additionally, the time stability of d_{33} for the hexagonal-shaped structure was measured, and the results are presented in Table 6. The time stability of d_{33} is highly dependent on the electret properties of the applied foil. Thus, further research on the electret properties of biodegradable foils is recommended.

5. Conclusions

In this study, a biodegradable piezoelectric transducer composed of polylactide (PLA) and natural rubber (NR) was presented. The metal ring prevents the electret foil from moving and provides an electrical connection between the metalized part of the foil and the output (measuring electrode). The application of 3-D printing methods allows prefabricating transducers in any shape and dimensions limited only by the printer resolution. Moreover, the presented design allows the application of different biodegradable and non-biodegradable materials as particular layers to optimize the properties according to the proposed model. Not only natural rubber, but also various biodegradable elastic dielectrics, can be applied to enhance the piezoelectric properties of the transducer.

Another crucial element influencing the piezoelectric response is the biodegradable foil, which should indicate sufficient electret properties. The results demonstrated that PLA, despite having a lower (even two orders of magnitude) Maxwell-time constant compared to traditional electret materials like PTFE and PP, exhibits sufficient electret properties to serve as a functional dielectric layer in piezoelectric applications. Further research on PLA is essential, including the influence of charging voltage, charging time, and external conditions on charge decay characteristics. The increase in charging voltage may lead to the rise of effective charge density, but also to faster charge decay, which is not desired for electret applications. Moreover, the PLA composites could be examined for possible application as an electret material.

The experimental findings confirmed that the shape of the dielectric mesh significantly impacts the transducer's electromechanical properties. Due to static measurements, the higher piezoelectric coefficient d_{33} was obtained for the hexagonal-shaped structure (224 pC/N) than for the stripped one (138 pC/N). The calculated results are about 85% lower than the calculated ones. The increase in piezoelectric response is possible due to optimisation of charging properties, especially an increase in charging voltage.

The measured piezoelectric coefficient is pressure-dependent in the range from 1.5 to 15 kPa. The reason can be the non-linear stress-strain characteristic of the applied natural rubber. The application of different coating materials could enhance the mechanical properties of the sample.

Overall, the results highlight the potential of PLA-based piezoelectric transducers for environmentally friendly applications, including energy harvesting, wearable electronics, and biomedical sensors. Future research should focus on optimization of the geometry, exploring alternative biodegradable materials with higher resistivity, and examining biodegradable elastic materials for enhancement of mechanical properties of the whole transducer.

References

- [1] Ali M., Bathaei M.J., Istif E., Karimi S.N.H., Beker L., *Biodegradable Piezoelectric Polymers: Recent Advancements in Materials and Applications*, Advanced Healthcare Materials, vol. 12, no. 23, pp. 1–32 (2023), DOI: 10.1002/adhm.202300318.
- [2] Panda S., Hajra S., Mistewicz K., In-na P., Sahu M., Rajaitha P.M., Kim H.J., *Piezoelectric energy harvesting systems for biomedical applications*, Nano Energy, vol. 100, no. April, 107514 (2022), DOI: 10.1016/j.nanoen.2022.107514.
- [3] Maamer B., Jaziri N., Said M.H., Tounsi F., *High-displacement electret-based energy harvesting system for powering leadless pacemakers from heartbeats*, Archives of Electrical Engineering, vol. 72, no. 1, pp. 229–238 (2023), DOI: 10.24425/aee.2023.143699.
- [4] Altmann A.A., Souissi F., Ben Dali O., Suppelt S., Latsch B., Dorsam J.H., Zhukov S., Flachs D., Kupnik M., Flexible 3D Printed Ferroelectret Sensors Integrated into Smart Textiles for Unobtrusive Monitoring, FLEPS 2024 IEEE International Conference on Flexible and Printable Sensors and Systems, Tampere, Finland (2024), DOI: 10.1109/FLEPS61194.2024.10604067.
- [5] Hayano J., Yamamoto H., Tanaka H., Yuda E., *Piezoelectric rubber sheet sensor: a promising tool for home sleep apnea testing*, Sleep and Breathing, vol. 28, no. 3, pp. 1273–1283 (2024), DOI: 10.1007/s11325-024-02991-9.
- [6] Zhang J., Li R., Dong L., Ke Y., Liu C., Pei M., Hu K., Ruan J., Li J., Yang F., Ultrasensitive biodegradable piezoelectric sensors with localized stress concentration strategy for real-time physiological monitoring, Chemical Engineering Journal, vol. 507, no. January, 160521 (2025), DOI: 10.1016/j.cej.2025.160521.
- [7] Ben Achour M.A., Rguiti M., Samuel C., Barrau S., Lacrampe M.-F., Courtois C., Energy harvesting by uniaxially-stretched poly (lactide) films at low tensile strain frequencies for powering wearable sensors: experimental results and theoretical extrapolation, Smart Materials and Structures, vol. 32, no. 075009, pp. 1–14 (2022), DOI: 10.1088/1361-665X/acd972.
- [8] Kacprzyk R., Grygorcewicz A., *Piezoelectric transducer*, Polish Patent PL no. 230284 (2018).
- [9] Qiu X., Gerhard R., Mellinger A., *Turning polymer foams or polymer-film systems into ferroelectrets: Dielectric barrier discharges in voids*, IEEE Transactions on Dielectrics and Electrical Insulation, vol. 18, no. 1, pp. 34–42 (2011), DOI:

10.1109/TDEI.2011.5704490.

- [10] von Seggern H., Zhukov S., Dali O. Ben, Hartmann C., Sessler G.M., Kupnik M., *Highly Efficient Piezoelectrets through Ultra-Soft Elastomeric Spacers*, Polymers, vol. 13, no. 21, 3751 (2021), DOI: 10.3390/polym13213751.
- [11] Mirkowska A., Fabrication and properties of sandwich dielectric structures with piezoelectric response, IEEE Transactions on Dielectrics and Electrical Insulation, vol. 31 no. 5, pp. 2275–2282 (2024), DOI: 10.1109/TDEI.2024.3398573.
- [12] Mirkowska A., Kacprzyk R., Rozmaryniewicz K., *Piezoelectric Structure with a 3-D Printed Mesh Layer*, IEEE Transactions on Dielectrics and Electrical Insulation, vol. 29, no. 3, pp. 823–828 (2022), DOI: 10.1109/TDEI.2022.3168366.
- [13] Sellami Y., Ben Dali O., Chadda R., Zhukov S., Guermazi M., Altmann A.A., von Seggern H., Latsch B., Schafer N., Kupnik M., *Piezoelectret Sensors from Direct 3D-Printing onto Bulk Films*, Proceedings of IEEE Sensors, Vienna, Austria (2023), DOI: 10.1109/SENSORS56945.2023.10324862.
- [14] Electrical Properties of Plastic Materials, [online], available: https://www.professionalplastics.com/professionalplastics/ElectricalPropertiesofPlastic s.pdf?srsltid=AfmBOorrQrwZdDDWFMifispZPenALfwhNh7M0KA15C4vOzVFDD OfNUb2, accessed: January 2025.
- [15] Sessler G.M., *Electrets*, Berlin: Springer-Verlag Berlin (1987), DOI: 10.1007/3-540-17335-8.
- [16] Gerhard-Multhaupt R., *Less can be more*, IEEE Transactions on Dielectrics and Electrical Insulation, vol. 9, no. 5, pp. 850–859 (2002), DOI: 10.7748/ns.16.7.24.s40.
- [17] Ansari M.A., Somdee P., *Piezoelectric Polymeric Foams as Flexible Energy Harvesters: A Review*, Advanced Energy and Sustainability Research, vol. 3, no. 9 (2022), DOI: 10.1002/aesr.202200063.
- [18] Moreira M.M.A.C., Soares I.N., Assagra Y.A.O., Sousa F.S.I., Nordi T.M., Dourado D.M., Gounella R.H., Carmo J.P., Altafim R.A.C., Altafim R.A.P., *Piezoelectrets: A Brief Introduction*, IEEE Sensors Journal, vol. 21, no. 20, pp. 22317–22328 (2021), DOI: 10.1109/JSEN.2021.3096424.
- [19] Mohebbi A., Mighri F., Ajji A., Rodrigue D., *Cellular Polymer Ferroelectret: A Review on Their Development and Their Piezoelectric Properties*, Advances in Polymer Technology, vol. 37 no. 2, pp. 1–16 (2016), DOI: 10.1002/adv.21686.
- [20] Perna G., Bonacci F., Caponi S., Clementi G., Di Michele A., Gammaitoni L., Mattarelli M., Neri I., Puglia D., Cottone F., *3D-Printed Piezoelectret Based on Foamed Polylactic Acid for Energy-Harvesting and Sensing Applications*, Nanomaterials, vol. 13, no. 22, pp. 1–15 (2023), DOI: 10.3390/nano13222953.
- [21] Urbaniak-Domagala W., *Electrical properties of polylactides*, Journal of Electrostatics, vol. 71, no. 3, pp. 456–461 (2013), DOI: 10.1016/j.elstat.2013.01.008.
- [22] Kamalova R.I., Minzagirova A.M., Galikhanov M.F., Spiridonova R.R., Guzhova A.A., Khairullin R.Z., *Electret properties of polylactic acid Montmorillonite composites*, AIP Conference Proceedings, vol. 2174, no. 020026 (2019), DOI: 10.1063/1.5134177.
- [23] Zagidullina I.A., Galikhanov M.F., Kamalova R.I., Sharipova G.F., Khairullin R.Z., *The study of the electret properties of polylactic acid and mineral fillers*, AIP Conference Proceedings, vol. 2313, no. 050048 (2020), DOI: 10.1063/5.0033479.

- [24] Flachs D., Zhukov S., Zech I., Schreck T., Belle S., von Seggern H. *et al.*, *Enzymatic Self-Degradable PLA-Based Electrets*, Journal of Polymers and the Environment, vol. 32, pp. 3922–3932 (2024) DOI: 10.1007/s10924-024-03240-6.
- [25] Zhukov S., Ma X., von Seggern H., Sessler G.M., Dali Omar Ben, Kupnik M., Zhang X., Biodegradable cellular polylactic acid ferroelectrets with strong longitudinal and transverse piezoelectricity, Applied Physics Letters, vol. 117, no. 11 (2020), DOI: 10.1063/5.0023153.
- [26] Altmann A.A., Suppelt S., Ruhl M., Schaumann S., Latsch B., Dali Omar Ben, Zhukov S., Flachs D., Zhang X., Thielemann C., von Seggern H., Kupnik M., Monolithic Wideband Air-Coupled Ultrasonic Transducer Based on Additively Manufactured Ferroelectrets, 2024 IEEE Ultrasonics, Ferroelectrics, and Frequency Control Joint Symposium (UFFC-JS), Taipei, Taiwan, pp. 1–4 (2024), DOI: 10.1109/UFFC-JS60046.2024.10793858.
- [27] Ma X., Qin Y., Zhou L., Hu Q., Xiang X., von Seggern H., Zhukov S., Altmann A.A., Kupnik M., Niu W., Zhang X., *Fully degradable, highly sensitive pressure sensor based on bipolar electret for biomechanical signal monitoring*, Materials Today Physics, vol. 49, no. November, 101597 (2024), DOI: 10.1016/j.mtphys.2024.101597.
- [28] Kacprzyk R., Motyl E., Gajewski J.B., Pasternak A., *Piezoelectric properties of nonuniform electrets*, Journal of Electrostatics, vol. 35, no. 2–3, pp. 161–166 (1995), DOI: 10.1016/0304-3886(95)00034-8.
- [29] Timoshenko S., Woinowsky-Krieger S., *Theory of plates and shells*. McGraw-Hill Book Company (1987), DOI: 10.1016/0006-8993(74)90278-9.
- [30] Puszczykowska N., Rytlewski P., Macko M., Fiedurek K., Janczak K., *Riboflavin as a Biodegradable Functional Additive for Thermoplastic Polymers*, Environments MDPI, vol. 9, no. 5 (2022), DOI: 10.3390/environments9050056.
- [31] Zhukov S., Eder-Goy D., Fedosov S., Xu B.-X., von Seggern H., *Analytical prediction of the piezoelectric d33 response of fluoropolymer arrays with tubular air channels*, Scientific Reports, vol. 8, no. 1, pp. 1–10 (2018), DOI: 10.1038/s41598-018-22918-1.
- [32] Hilczer B., Małecki J., *Electrets and piezopolymers (in Polish)*, Warszawa: Wydawnictwo Naukowe PWN (1992).
- [33] Lisowski M., Measurements of resistivity and dielectric permittivity of solid dielectrics (in Polish), Wrocław: Oficyna Wydawnicza Politechniki Wrocławskiej (2004).
- [34] Kacprzyk R., Mirkowska A., *Piezo-tubes*, IEEE Transactions on Dielectrics and Electrical Insulation, vol. 25, no. 3 (2018), DOI: 10.1109/TDEI.2017.006899.
- [35] Mellinger A., Charge Storage in Electret Polymers: Mechanisms, Characterization and Applications, Universitat Potsdam (1967).
- [36] Rychkov D., Kuznetsov A., Rychkov A., Electret properties of polyethylene and polytetrafluoroethylene films with chemically modified surface, IEEE Transactions on Dielectrics and Electrical Insulation, vol. 18, no. 1, pp. 8–14 (2011), DOI: 10.1109/TDEI.2011.5704487.